Physics of Plasmas

Formation of the radio frequency sheath of plasma with Cairns–Tsallis electron velocity distribution

Cite as: Phys. Plasmas **27**, 083517 (2020); https://doi.org/10.1063/5.0015346
Submitted: 27 May 2020 . Accepted: 20 July 2020 . Published Online: 11 August 2020

Jing Ou, and Zongzheng Men

View Online Export Citation CrossMark

ARTICLES YOU MAY BE INTERESTED IN

Numerical investigation of secondary electron emission effect on the dusty plasma sheath with superextensive electrons
Physics of Plasmas **27**, 083701 (2020); https://doi.org/10.1063/5.0010080

Announcement: The 2019 James Clerk Maxwell Prize for Plasma Physics
Physics of Plasmas **27**, 080201 (2020); https://doi.org/10.1063/5.0020008

New insights into the physics of rotating spokes in partially magnetized $E \times B$ plasmas
Physics of Plasmas **27**, 083520 (2020); https://doi.org/10.1063/5.0014357

AIP Publishing

© 2020 Author(s).

Physics of Plasmas ARTICLE scitation.org/journal/php

Formation of the radio frequency sheath of plasma with Cairns–Tsallis electron velocity distribution

Cite as: Phys. Plasmas **27**, 083517 (2020); doi: 10.1063/5.0015346
Submitted: 27 May 2020 · Accepted: 20 July 2020 ·
Published Online: 11 August 2020

View Online Export Citation CrossMark

Jing Ou[1,2,a)] and Zongzheng Men[1]

AFFILIATIONS

[1]Institute of Plasma Physics, Chinese Academy of Sciences, Hefei 230031, China
[2]Center for Magnetic Fusion Theory, Chinese Academy of Sciences, Hefei 230031, China

[a)]Author to whom correspondence should be addressed: ouj@ipp.ac.cn

ABSTRACT

The effect of the non-Maxwellian plasma with enhanced electron tails on the properties of the radio frequency (RF) sheath is studied with a one-dimensional collisionless model, which consists of the sheath model and the equivalent circuit model. In the sheath model, electrons are assumed to obey the Cairns–Tsallis distribution. For various entropic indices q characterizing the degree of electron nonextensivity and parameter α measuring the electron nonthermality state, the electron nonextensivity and nonthermality are found to modify the potential drop across the sheath and the sheath thickness, as well as the spatiotemporal variations of the potential, the ion and electron densities inside the sheath. With the decrease in q and the increase in α, the potential drop across the sheath and the thickness increase at any time in a RF cycle as a result of the increase in superthermal electrons in the non-Maxwellian tail. The dependence of the potential drop across the sheath on q and α is deeply related to the frequency and amplitude of the disturbance current. When the electron nonextensivity and nonthermality are strengthened, the enhancement of the sheath potential drop can cause a significant increase in the ion bombardment energy on the wall, sheath power dissipation, and plasma energy flux to the wall.

Published under license by AIP Publishing. https://doi.org/10.1063/5.0015346

I. INTRODUCTION

Radio frequency (RF) sheaths play an important role in edge plasma properties and plasma–wall interactions in a wide variety of plasma fields. In fusion experiments, RF sheaths driven by ion cyclotron range of frequency (ICRF) waves on the antenna and other boundary surfaces can sometimes cause strong RF-enhanced impurity sputtering and self-sputtering, parasitic power dissipation, hot spots, and reduced heating efficiency of the core plasma.[1] In the microelectronics industry, the RF biased sheath of the electrode where the wafer is placed determines the magnitude of ion bombardment energy on the wafer in etching and deposition during material processing.[2] Accordingly, the formation of the RF sheath has been studied by using numerical, analytical, and semi-analytical models.[1–10] In most of these works, the fully fluid approximation[3,4] or the simple Boltzmann distribution[1,2,5–10] was used to describe the electron profile in the sheath based on the electrons in the state of local thermal equilibrium.

In the fusion plasma, astrophysics plasma and laboratory plasma, it is the common phenomenon that the presence of energetic electrons makes the electron distribution non-equilibrium and some deviation from the Maxwellian. To investigate the effect of the energetic electrons on the sheath structure and the resultant plasma–wall interaction, different sheath models have been proposed for the electrostatic or RF sheath.[11–22] The typical method is approximated by the sum of two electron distributions:[11–18] the thermal Maxwellian background and a small suprathermal population. In Ref. 11, with the assumption of small energetic electrons via the phenomenological modification to the Maxwellian background electron distribution, the structure of the RF sheath in the presence of a monoenergetic electron beam has been examined. It is found that even small beam flux can lead to the enhancement of the sheath potential drop at any time in an RF cycle. Another common method is that the electrons in non-equilibrium are described by only one non-Maxwellian electron velocity distribution function.[19–22] Based on a generalization of the Boltzmann–Gibbs–Shannon (BGS) system,[23] Tsallis proposed a model in which a parameter q characterizes the degree of nonextensivity of the velocity distribution. $-1 < q < 1$ denotes the long-tailed distribution function with an excess of energetic particles, and $q > 1$ represents the distribution function exhibiting a thermal cutoff on the maximum value allowing for the particle velocity. The Tsallis model, connected to the well known κ distribution with a formal transformation $\kappa = 1/(1-q)$,[24] has been used to investigate the formation of the non-Maxwellian electron plasma sheath.[16,20] In order to model the

Published under license by AIP Publishing

superthermal particles, Cairns *et al.* introduced a model with a parameter α set to characterize the deviation from the Maxwellian distribution caused by the enhanced high-energy tails.[25] Tribeche *et al.*[26] have proposed a hybrid Cairns–Tsallis distribution function, which purports to offer enhanced parametric flexibility in modeling non-thermal plasmas with two parameters q and α. Cairns–Tsallis distribution is a physically meaningful model since it can adjust two parameters to fit the wider range of observed plasmas. By employing Cairns–Tsallis velocity distribution, there have been many theoretical investigations of the basic plasma property,[21,28–33] including the effect of the interaction of nonthermality and nonextensivity on the Debye shielding in an electrostatic sheath.[21]

In this paper, we use the Cairns–Tsallis distribution function to describe electrons with enhanced high-energy tails in a RF sheath of fusion plasma and then investigate the effect of the electron nonthermality and nonextensivity on the sheath structure and the related ion bombardment energy on the wall, sheath power dissipation, and total plasma energy flux to the wall. The rest of this paper is organized as follows. The model description is presented in Sec. II. Section III shows the numerical results and discussion. The conclusion is given in Sec. IV.

II. MODEL DESCRIPTION

During simultaneous ICRF wave heating and lower hybrid wave heating operation in tokamak, the energetic electrons caused by the lower hybrid wave heating make the electrons deviate from the Maxwellian distribution and then can affect the RF sheath driven by the ICRF wave. Here, Cairns–Tsallis distribution is used to describe the non-Maxwellian electrons with enhanced tails, while the ions are described by the fluid equations. As shown in Fig. 1, the RF sheath is driven by a current disturbance with ICRF ω at the wall, and a one-dimensional collisionless and unmagnetized sheath is considered. At any time t, $x = 0$ is the wall position and plasma-sheath edge is at $x = ds(t)$, where ds denotes the time-dependent sheath thickness. For the sheath consisting of singly charged ions and electrons, the spatiotemporal variation of the sheath potential $\phi(x,t)$ is described by the Poisson equation,

$$\frac{\partial^2\phi}{\partial x^2} = -\frac{e}{\varepsilon_0}(n_i - n_e), \tag{1}$$

where e, ε_0, $n_i(x,t)$, and $n_e(x,t)$ are the elementary charge, the permittivity of free space, and the spatiotemporal variation of the ion and electron densities, respectively. At $x = ds(t)$, $\phi(ds,t)$ is assumed to be approximately zero, i.e., $\phi(ds,t) = 0$, and the plasma satisfies the quasi-neutral condition $n_{i,0} = n_{e,0} = n_0$. For the electrons, the one-dimensional hybrid Cairns–Tsallis velocity distribution function is written as[26]

$$f_{q,\alpha}(v) = C_{q,\alpha}\left(1 + \alpha\frac{v^4}{v_{te}^4}\right)\left[1 - (q-1)\frac{v^2}{2v_{te}^2}\right]^{1/(q-1)}, \tag{2}$$

where $v_{te} = (k_B T_e/m_e)^{1/2}$ is the electron thermal velocity with k_B being the Boltzmann constant, T_e the electron temperature for Maxwellian distribution, and m_e the electron mass. q and α are the parameters associated with the electron nonextensivity and nonthermality, respectively. It was pointed out by Verheest and Pillay that the pure Cairns distribution function develops wings and may become unstable for $\alpha > 0.25$.[34] Williams *et al.* restricted the domain of allowable nonextensive parameters to the range of $0.6 < q < 1$, involving high-energy non-Maxwellian tails.[27] For $0.6 < q < 1$, the constant parameter[26]

$$C_{q,\alpha} = n_{e0}\sqrt{\frac{m_e}{2\pi k_B T_e}}\frac{\Gamma\left(\frac{1}{1-q}\right)(1-q)^{5/2}}{\Gamma\left(\frac{1}{1-q}-\frac{5}{2}\right)\left[3\alpha + \left(\frac{1}{1-q}-\frac{3}{2}\right)\left(\frac{1}{1-q}-\frac{5}{2}\right)(1-q)^2\right]}, \tag{3}$$

where Γ stands for the standard gamma function.

In tokamaks such as EAST, the applied ICRF ω is in the 20–70 MHz range. For the typical edge plasma density n_0 in the range of 10^{17}–10^{18} m^{-3}, the electron plasma frequency $\omega_{pe} = \sqrt{n_{e,0}e^2/m_e\varepsilon_0}$ is about 10^3–10^4 MHz. Since $\omega \ll \omega_{pe}$, the electrons can respond to the instantaneous sheath potential. Integrating the electron distribution function in the sheath over the velocity spaces gives the profile of the electron density in the sheath,[26,27]

$$n_e(x,t) = n_{e0}\left[1 + (q-1)\frac{e\phi(x,t)}{k_B T_e}\right]^{1/(q-1)+1/2} \times \left[1 + A\frac{e\phi(x,t)}{k_B T_e} + B\left(\frac{e\phi(x,t)}{k_B T_e}\right)^2\right], \tag{4}$$

where $A = -16q\alpha/(3 - 14q + 15q^2 + 12\alpha)$ and $B = 16(2q-1)q\alpha/(3 - 14q + 15q^2 + 12\alpha)$.

The ion continuity and momentum equations are employed for the ion fluid to obtain the ion density

$$\frac{\partial n_i}{\partial t} + \frac{\partial(n_i v_i)}{\partial x} = 0, \tag{5}$$

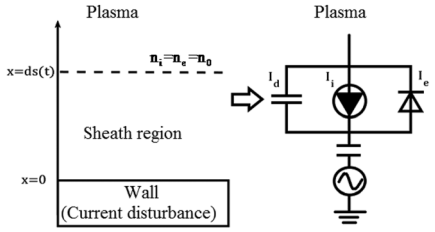

FIG. 1. RF sheath model geometry and the equivalent circuit model.

Published under license by AIP Publishing

$$\frac{\partial v_i}{\partial t} + v_i \frac{\partial v_i}{\partial x} = -\frac{e}{m_i}\frac{\partial \phi}{\partial x} - \frac{1}{m_i n_i}\frac{\partial p_i}{\partial x}, \tag{6}$$

where m_i and v_i are the ion mass and velocity, respectively. The pressure term $p_i = n_i k_B T_i$ with the ion temperature T_i. Even for a RF sheath, ion velocity satisfies the Bohm criterion at the plasma-sheath edge,[35,36] and it can be written as $v_{i0} \geq C_s = \sqrt{(T_{scr} + \gamma T_i)/m_i}$,[37] where γ is the ion polytropic coefficient. $T_{scr} = 2T_e/(1+q+2A)$ is the electron screening temperature, obtained from $T_{scr} = \frac{en_e(\phi)}{dn_e/d\phi}|_{\phi=0}$. We can see that the ion velocity entering the sheath is related not only to the temperature but also to the electron distribution. C_s increases with the decrease in q and the increase in α, as discussed in Refs. 21 and 27. In the following discussion, we only consider $v_{i0} = C_s$, i.e., Bohm criterion in a marginal form.

The system equations can be solved if the sheath potential at the wall $\phi(0,t)$ is known. However, even if a sinusoidal RF current source is applied on the wall, the sheath potential near the wall is not exactly sinusoidal due to the effect of sheath loading.[6] In fact, both the forms and amplitudes of the sheath potential at the wall should be determined self-consistently by the current balance condition on the wall.[38] To obtain $\phi(0,t)$, an equivalent circuit model is introduced to determine self-consistently the instantaneous relationship between $ds(t)$ and $\phi(0,t)$.[6,8–11] As shown in Fig. 1, the sheath is modeled as a parallel combination of a diode, a capacitor, and a current source. The ion current incident onto the wall is expressed by

$$I_i(t) = eA_s J_i(0,t), \tag{7}$$

where A_s is the wall area and $J_i(0,t) = v_i(0,t)n_i(0,t)$ is the ion flux to the wall.

The current through the diode represents the variation of the electron current can be written as

$$I_e(t) = eA_s J_e(0,t), \tag{8}$$

where $J_e(0,t)$ is the electron flux for the Cairns–Tsallis distribution at the wall.[32]

$$J_e(0,t) = A_1 \frac{1}{q}\left[1 + (q-1)\frac{e\phi(0,t)}{k_B T_e}\right]^{q/(q-1)} \times \left[1 + B_1 \frac{e\phi(0,t)}{k_B T_e}\left(\frac{e\phi(0,t)}{k_B T_e} + \frac{2q}{2q-1}\right)\right], \tag{9}$$

where $A_1 = C_{q,\alpha}\frac{k_B T_e}{m_e}\frac{8\alpha+(3q-2)(2q-1)}{(3q-2)(2q-1)}$ and $B_1 = \frac{4\alpha q(2q-1)}{8\alpha+(3q-2)(2q-1)}$.

The displacement current caused by the time variation of the charge Q at the wall is

$$I_d(t) = \frac{dQ}{dt} = C_{cap}\frac{d\phi(0,t)}{dt} + \phi(0,t)\frac{dC_{cap}}{dt}, \tag{10}$$

where $C_{cap} = \varepsilon_0 A_s/ds(t)$ is the time-dependent sheath capacitance. With the assumption that disturbance current in ICRF applied at the wall is sinusoidal, the current balance equation can be written as

$$I_i(t) - I_e(t) - I_d(t) = I_{\max}\sin(\omega t), \tag{11}$$

where $I_{\max}$ is the amplitude of the disturbance current.

For convenience, the following dimensionless quantities are introduced: $N_i = n_i/n_0$, $N_e = n_e/n_0$, $\varphi = e\phi/k_B T_e$, $u_i = v_i/\sqrt{k_B T_e/m_i}$, $f_b = \omega/\omega_{pi}$ with ion plasma frequency $\omega_{pi} = \sqrt{n_{i,0}e^2/m_i\varepsilon_0}$, and the RF cycle $\tau = t/t_0$ with $t_0 = 2\pi/\omega_{pi}$. In our calculation, Eqs. (1) and [(5) and (6)] are solved through a second order finite difference scheme in space and an explicit scheme in time, and the iteration method is used to solve numerically a set of closed nonlinear equations with the boundary conditions. The algorithm is as follows: the initial $ds(t)$, $u_i(0,t)$, and $N_i(0,t)$ are guessed and the constant sheath capacitance is assumed, then Eq. (10) are solved after Eq. (11) is substituted ion to Eq. (10) to obtain the $\varphi(0,t)$ for a given $I_{\max}$ by using the fourth-order Runge–Kutta method. With the obtained $\varphi(0,t)$ and sheath potential waveform, Eqs. (1) and (4)–(6) are solved to obtain the new $ds(t)$, $u_i(0,t)$, and $N_i(0,t)$. The iteration is repeated until the solutions converge to a self-consistent periodic steady state.[6–8]

III. RESULTS AND DISCUSSION

In this section, we present and discuss the results obtained from the model equations for fusion plasma. The deuterium is considered as the only discharge gas. With the assumption of electrons in near-Maxwellian state, $0 < \alpha < 0.01$ and $0.75 < q < 1$ are taken into account for the Cairns–Tsallis distribution. The following parameters are chosen from the current typical parameters at EAST-like tokamak during ICRF wave heating as default parameters: $T_i = T_e = 10$ eV, $n_0 = 2.5 \times 10^{17}$ m^{-3}, $A_s = 0.8$ m^2, $f_b = 0.5$, $I_{\max} = 1000$ A, $\alpha = 0.001$, and $q = 0.8$.

In an electrostatic sheath, it is shown that the sheath thickness and sheath potential increase as the electron nonextensivity or nonthermality strengthens.[16,21] Here, we first investigate variations of the sheath thickness and sheath potential at the wall as a function of time in two RF cycles for different q and α. As shown in Fig. 2, for a positive disturbance current at the wall in the first half of the cycle, the waveforms of sheath potential and sheath thickness have a large excursion in some part, the sheath potential drop reaches its maximum, and the sheath thickness also reaches its maximum. For a negative disturbance current at the wall in the latter half of the cycle, the waveforms of the sheath potential and sheath thickness become gentle and the sheath potential drop and sheath thickness are small in most part. These results are in good agreement with those of Ref. 11 in which the energetic electron component is taken into account. With the decrease in q

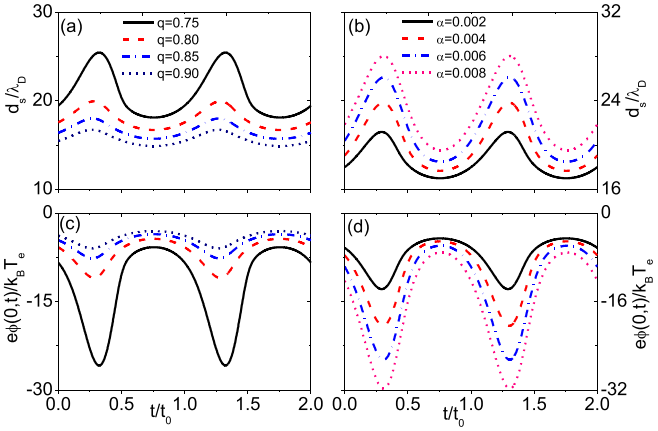

FIG. 2. The sheath thickness normalized by Debye length $\lambda_D = \sqrt{\varepsilon_0 k_B T_e/n_0 e^2}$ [(a) and (b)] and the sheath potential at the wall normalized by temperature $k_B T_e$ [(c) and (d)] in two cycles for different q [(a) and (c)] and for different α [(b) and (d)]. The other parameters are set to their defaults.

Published under license by AIP Publishing

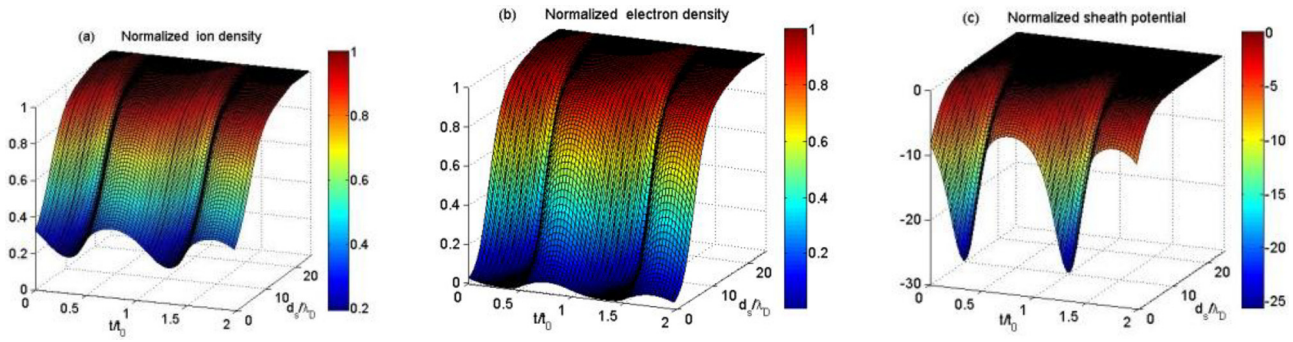

FIG. 3. The spatiotemporal variations of (a) the normalized ion density, (b) the normalized electron density inside the sheath, and (c) the normalized sheath potential for $q = 0.75$ in two cycles. The other parameters are set to their defaults.

and increase in α, the sheath potential drop and the sheath thickness increase at any time in a cycle. The dependence of the sheath potential drop and sheath thickness on q and α is more significant in the first half of the cycle than in the latter half of the cycle, and the sheath potential increases the most in the maximum of the sheath potential drop. This is due to the fact that the sheath potential is always negative in a capacitive sheath to keep the current balance at the wall.[6] For a positive disturbance current at the wall, the sheath potential drop becomes so large that almost thermal electrons are reflected before they reach the wall and most of the energetic electrons can reach the wall in the first half of the cycle. As a result, even a small increase in the energetic electron can change the time variation of the charge at the wall and the resultant sheath potential drop because the sheath current balance is dominated by the displacement current and the electron current which is induced by energetic electrons. In the latter half of the cycle, the disturbance current becomes negative and it can be balanced by the ion and the electron currents. The sheath potential is modified by the energetic electrons but the increase is not significant for the electron in the near-Maxwellian state. The reason is that the sheath potential drop is sufficient, and then most of the thermal and the energetic electrons can reach the wall. Under this condition, the current change caused by energy electrons has a little effect on the whole. From Fig. 2, it is found that the decrease in q and the increase in α can enhance the electron high-energy tail and cause the electron distribution function far from the Maxwellian distribution, which makes the increase in the sheath thickness and the sheath potential at any time. By investigation of the evolution of the sheath potential at the wall and the corresponding sheath thickness in two cycles, it is demonstrated that the effect of the electron nonextensivity and nonthermality on the sheath structure is more pronounced for smaller q and larger α. Our results also show that tendencies of the sheath thickness and sheath potential drop with electron nonextensivity or nonthermality in a RF sheath at any time are the same as in an electrostatic sheath shown in Refs. 16 and 21.

To scrutinize the effect of the electron nonextensivity on the sheath structure, we display the spatiotemporal variations of the ion and electron densities in the RF sheath region and sheath potential for two cases of $q = 0.75$ and $q = 0.95$ in Figs. 3 and 4. For the Maxwellian electron RF sheath, it is shown in Ref. 8 that the plasma density varies obviously with the spatial variable but gently with the time, and the sheath potential shows a significant spatial change near the wall and its temporal profile oscillates periodically with the time. For the non-Maxwellian electron RF sheath, ion and electron densities and sheath potential have similar spatiotemporal variations in the present work, as shown in Figs. 3 and 4. In a RF capacitive sheath in ICRF, the negative sheath potential exists all the time due to the current balance at the wall.[6] Therefore, the ion density decreases from the plasma-sheath edge to the wall because ions are accelerated across the sheath and then impact the wall, while the electrons are expelled away from the wall and leave the sheath to the bulk plasma rapidly. Due to

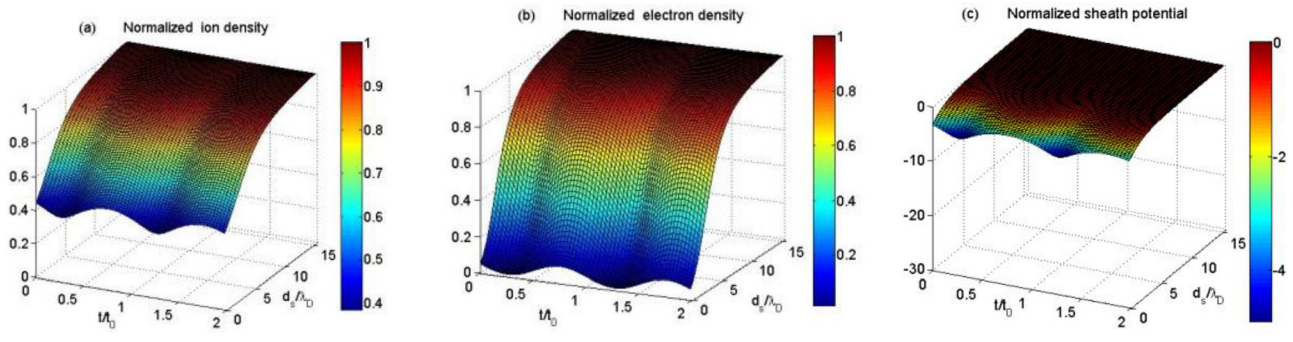

FIG. 4. The spatiotemporal variations of (a) the normalized ion density, (b) the normalized electron density inside the sheath, and (c) the normalized sheath potential for $q = 0.95$ in two cycles. The other parameters are set to their defaults.

Published under license by AIP Publishing

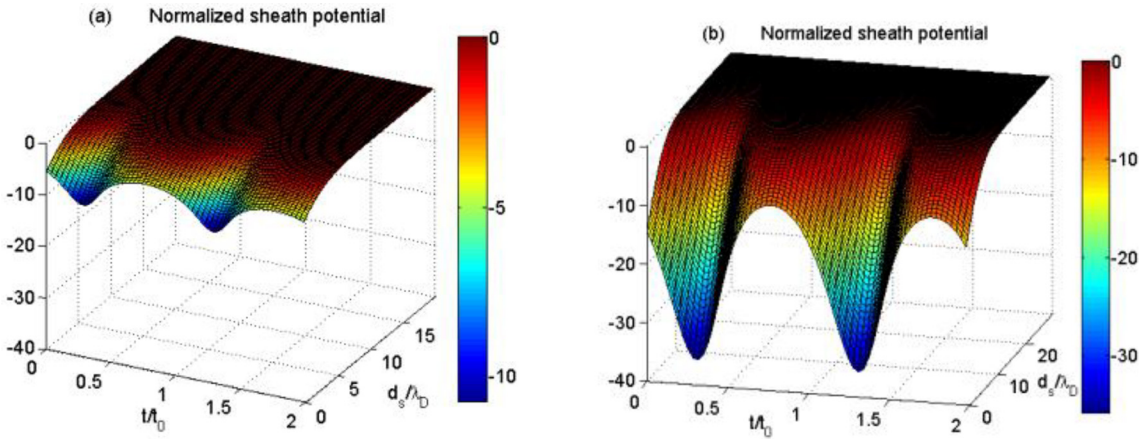

FIG. 5. The spatiotemporal variations of the normalized sheath potential in two cycles for (a) $\alpha = 0.001$ and (b) $\alpha = 0.01$. The other parameters are set to their defaults.

the large sheath potential drop and the thick sheath in the first half of the cycle, the accelerated ions reach the wall in a longer distance. Meanwhile, the reflected electrons increase and electrons reach hardly the wall. The opposite occurs in the latter half of the cycle, which corresponds to the small sheath potential drop and the thin sheath. By comparing profiles of the sheath potential and sheath thickness in Figs. 3 and 4, it is found that the potential drop across the sheath is larger and the sheath thickness is longer at any time in a RF cycle for small q. The tendency is reasonable because smaller q means a more number of electrons with high velocities enter the sheath and then cause the sheath potential drop to rise. Similar results are also obtained for the increase in the electron nonthermality. In Fig. 5, we only show the spatiotemporal variations of sheath potential for $\alpha = 0.001$ and $\alpha = 0.01$. The larger potential drop across the sheath and broader sheath thickness for $\alpha = 0.01$ than for $\alpha = 0.001$ can be found due to the contribution of the more enhanced high-energy electron tails to the electron current. It is also inferred that the gradients of the spatial profile of both the ion and the electron are steeper as the electron nonthermality becomes strong.

Next, we investigate the minimum and maximum of the sheath potential, the maximum of the sheath potential difference, and the average sheath potential in a cycle as a function of q and α, respectively. As shown in Fig. 6, for the maximum of the sheath potential (i.e., the minimum potential drop across the sheath) corresponding to a very thin sheath thickness, variation of the potential drop across the sheath falls slowly with the decrease in q or the increase in α. For the minimum of the sheath potential (i.e., the maximum potential drop across the sheath) where the sheath thickness is very thick, the potential drop across the sheath is also found to depend strongly on q and α, and its increase is far larger than the minimum of the sheath potential drop with the decrease in q and the increase in α. Furthermore, the maximum of the sheath potential difference increases. Figure 6 also shows the average potential drop across the sheath in a cycle. With the decrease in q and the increase in α, the average potential drop across the sheath in a cycle increases because the sheath potential drop always increases at any time in a cycle, as indicated in Fig. 2.

Now, we discuss the dependence of the sheath potential on the disturbance source parameters for different q and α. From Figs. 7 and 8,

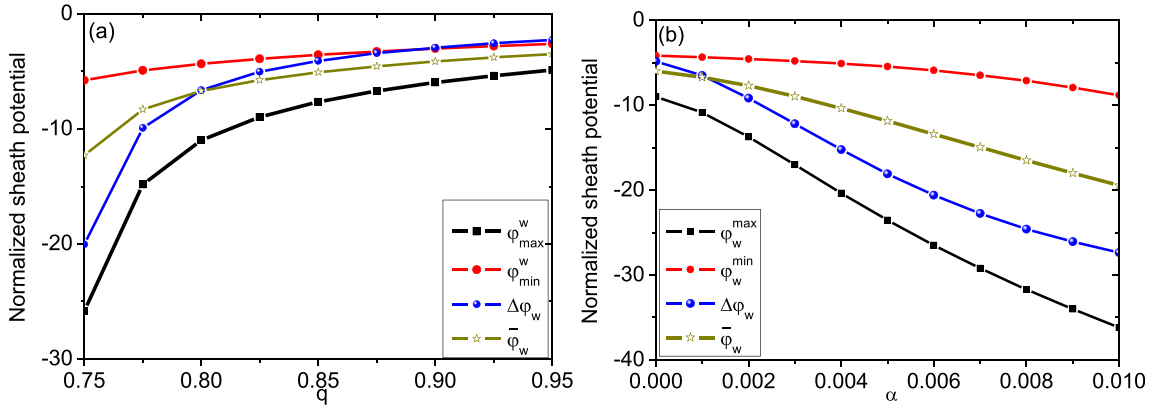

FIG. 6. The maximum and minimum of the sheath potential drop $\varphi_{max}(0,t)$ and $\varphi_{min}(0,t)$, the maximum of sheath potential difference $\Delta\varphi_w = \varphi_{max}(0,t) - \varphi_{min}(0,t)$, and the average sheath potential at the wall in a cycle $\bar{\varphi}_w = \frac{1}{\tau}\int_0^\tau \varphi(0,t)dt$ as a function of (a) q with $\alpha = 0.001$ and (b) α with $q = 0.8$. The other parameters are set to their defaults.

Published under license by AIP Publishing

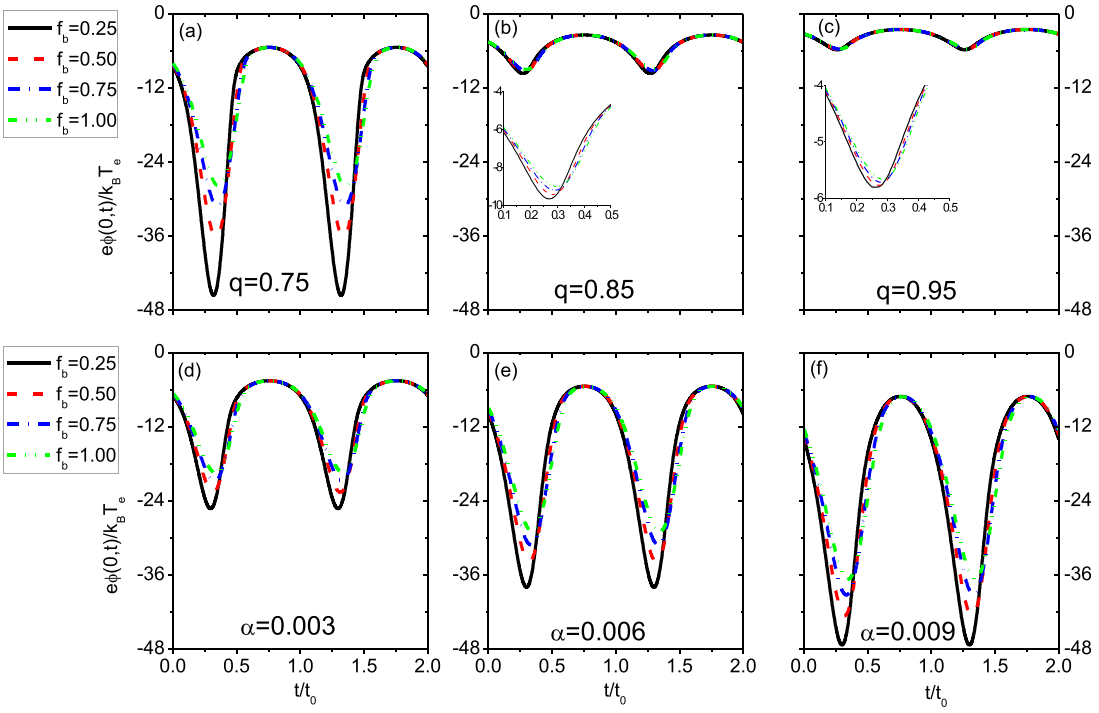

FIG. 7. The variation of the normalized sheath potential at the wall in two cycles for different normalized ICRFs of disturbance current with [(a)–(c)] different q and $\alpha = 0.001$ and [(d)–(f)] different α and $q = 0.8$. The other parameters are set to their defaults.

we can see that the amplitude and waveform of sheath potential are mainly determined by the disturbance source and modified by the non-Maxwellian electron distribution in ranges of our simulation parameters. The amplitude of the sheath potential decreases with the increase in the frequency, as reflected in the decrease in the maximum of the sheath potential drop. This result shown in Fig. 7 is in good agreement with that of Ref. 8 for the Maxwellian electron sheath. When taken into account electron nonextensivity, the variation of the sheath potential at the wall with frequency of disturbance current decreases with q and it tends to be almost independent of the frequency for the large q. When the electron nonthermality increases, the potential drop across the sheath increases. The increase in the sheath potential is found to be significant at the position where the sheath potential drop reaches its maximum. Figure 8 displays the effect the amplitude of the disturbance current on the sheath potential for different q and α. With an increase in the amplitude of the disturbance current, the sheath potential drop increases at the first half of the cycle, while it decreases at the latter half of the cycle. Although variation of sheath potential with the amplitude of the disturbance source is opposite at the first and the latter of the half cycles, the sheath potential drop shows a significant change in general with the decrease in q and the increase in α. The most significant change can be found at about the time when the sheath potential drop reaches its maximum. For the normalized time by the cycle, the time corresponding to the maximum of the sheath potential drop is almost the same for different q and α.

As an application of the model described in Sec. II, we discuss the effect of electron nonextensivity and nonthermality in tokamak plasma on impurity sputtering, heating efficiency, and hot spots via the ion bombardment energy on the wall, ion sheath power dissipation, and plasma energy flux to the wall. The RF sheath driven by the ICRF wave is of technological importance in tokamaks, and electron non-Maxwellian distribution with enhanced high-energy tails has been confirmed in the edge region during simultaneous ICRF wave heating and lower hybrid wave heating operation.[40,41] The ion bombardment energy on the wall E_i, ion sheath power dissipation P_{RF},[39] and plasma energy flux to the wall Q_{total} can be expressed as

$$E_i = 2k_B T_i + \frac{1}{2} m_i v_0^2 - e\phi(0,t), \tag{12}$$

$$P_{RF} = A_s J_i(0,t)\phi(0,t), \tag{13}$$

$$Q_{total} = J_i(0,t)\left[k_B T_i + \frac{1}{2} m_i C_s^2 - e\phi(0,t))\right] + J_e(0,t) T_{scr}. \tag{14}$$

With the decrease in q and the increase in α, the superthermal electrons in the non-Maxwellian tail are enhanced. Therefore, the ion velocity entering the sheath increases according to $T_{scr} = 2T_e/(1+q+2A)$[21,27] and the resultant ion flux increases, and what's more, the sheath potential drop increases, as shown in Figs. 2–5. From Fig. 9, we can see that the decrease in q and the increase in α can cause the increase in E_i, P_{RF}, and Q_{total}. Corresponding to the waveform of the sheath potential shown in Fig. 2, it is found that the variation of E_i, P_{RF}, and Q_{total} with q and α is mainly dominated by the potential drop across the RF sheath instead of the increase in the ion energy entering the sheath.

Published under license by AIP Publishing

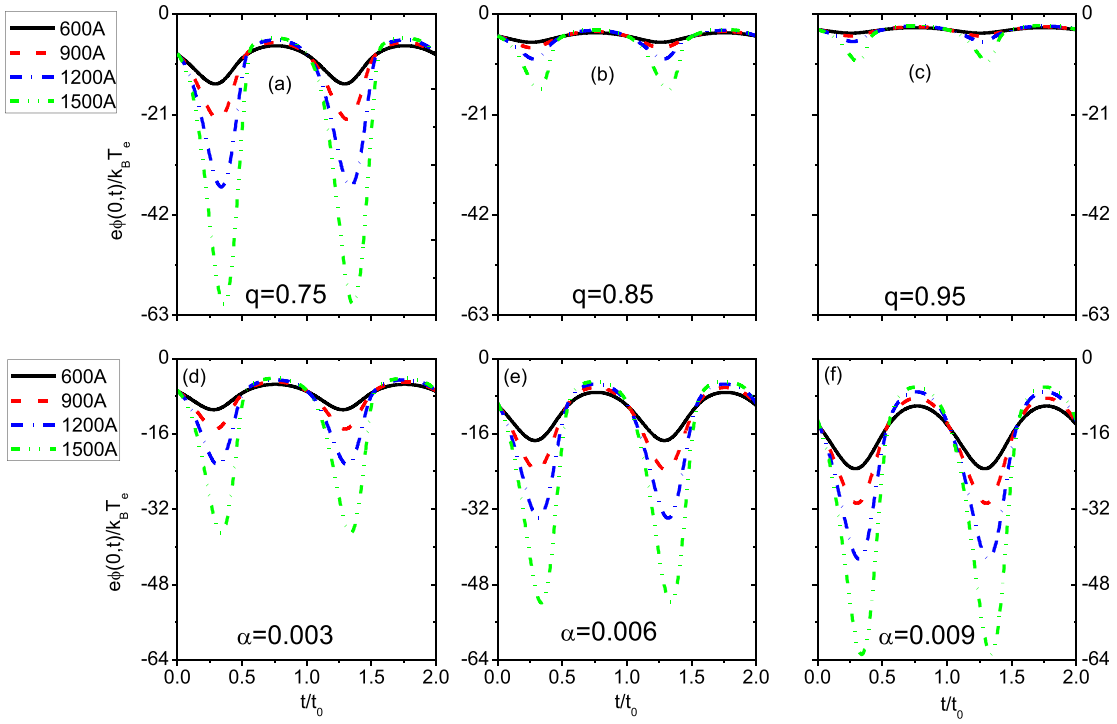

FIG. 8. The variation of the normalized sheath potential at the wall with time for different amplitudes of disturbance current with [(a)–(c)] different q and $\alpha = 0.001$ and [(d)–(f)] different α and $q = 0.8$. The other parameters are set to their defaults.

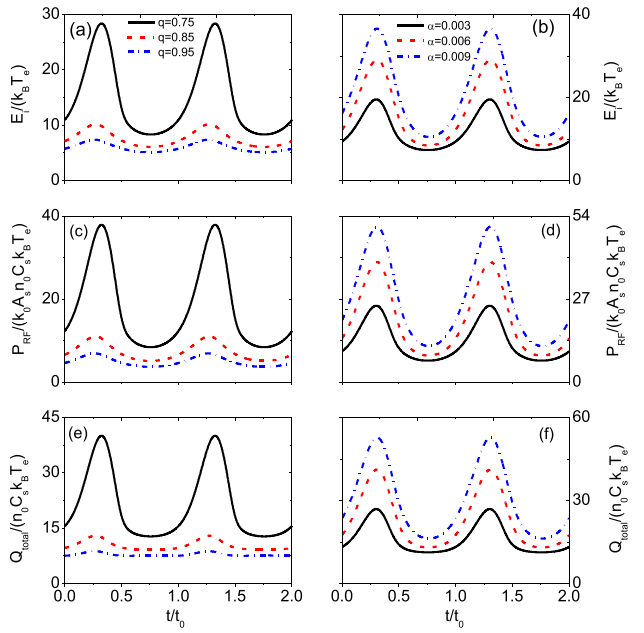

FIG. 9. The ion bombardment energy on the wall [(a) and (b)], the ion sheath power dissipation [(c) and (d)], and the total energy flux to the wall (e, f) in two cycles with different q and $\alpha = 0.001$ [(a), (c), and (e)] and with different α and $q = 0.8$ [(b), (d), and (f)]. The other parameters are set to their defaults. In [(c) and (d)], constant coefficient $k_0 = 1.5 \times 10^{-15}$ (Ref. 39).

IV. SUMMARY AND CONCLUSION

The one-dimensional collisionless hybrid model, consisting of the sheath model in the ion cyclotron range of frequencies and the equivalent circuit model, is used to study the properties of the radio frequency sheath of fusion plasma with enhanced non-Maxwellian electron tails. In the sheath model, ions are described by all the time-dependent terms in the fluid equations and non-Maxwellian electrons are assumed to obey the Cairns–Tsallis distribution. In the equivalent circuit model, the sheath is looked at as a parallel combination of a diode, a capacitor, and a current source. For various entropic index q characterizing the degree of electron nonextensivity and the parameter α measuring the electron nonthermality state, a set of equations describing the model are solved numerically to obtain the potential drop across the RF sheath and the sheath thickness, as well as the spatiotemporal variations of the potential, the ion and electron densities inside the sheath. Also, impacts of the variation of q and α on the ion bombardment energy on the wall, sheath power dissipation, and plasma energy flux to the wall are investigated.

It is shown that the potential drop across the sheath and the thickness increase at any time in a RF cycle with the decrease in q and the increase in α. In a cycle with sinusoidal current disturbance at the wall, the dependence of the sheath potential and sheath thickness on q and α is more pronounced during the positive disturbance current than during the negative disturbance current. The change of the sheath potential with q and α is found to be significant in the position where the sheath potential drop reaches its maximum. As shown from spatiotemporal variations of the plasma density and sheath potential, the ion and electron densities change obviously with spatial variable but

Published under license by AIP Publishing

gently with the time. The sheath potential shows a significant spatial change near the wall and its temporal profile oscillates periodically with time. As q is decreased or α is increased, the gradients of the spatial profile of both plasma density and sheath potential become steeper near the wall. For the decrease in q and the increase in α, both the maximum and minimum of the sheath potential drop increase, but the increase in the former is larger than that in the latter. As a result, the maximum of the sheath potential difference becomes larger. Moreover, the average sheath potential in the cycle also increases because the sheath potential drop always increases at any time in a cycle. The frequencies and amplitudes of the disturbance current can affect the variation of the potential drop across the sheath with q and α. As the disturbance current parameters are changed, the waveform of the sheath potential depends on q and α in a cycle, and the most significant change occurs at about the time when sheath potential drop reaches its maximum. For the normalized time by the cycle, the time corresponding to the maximum of the sheath potential drop is almost the same for different q and α.

The results should be of wide relevance to explain and interpret RF sheaths in the non-equilibrium fusion plasma related process. As an example, in EAST tokamak, it is found that the impurity source, lower heating efficiency, and heat load are modified by the RF sheath during simultaneous ICRF wave heating and lower hybrid wave heating operation.[40,41] The possible reason is that the superthermal electrons from the lower hybrid wave heating cause the enhancement of the RF sheath potential drop. The results presented in this work confirm that when the non-Maxwellian plasma with enhanced electron tails is presented, the ion bombardment energy on the wall, ion sheath power dissipation, and plasma energy flux to the wall always increase, which can affect the impurity sputtering, heating efficiency of the ICRF wave, and hot spot production on the material surface. Finally, it must be pointed out that the one-dimensional model is used to investigate the RF sheath structure in our present work. To further study the RF sheath of non-Maxwellian plasma with anisotropic velocity distribution, the particle-in-cell simulation framework such as Vsim software[42] should be carried out to include the three dimensional effect.

ACKNOWLEDGMENTS

This work was supported by the National Key R&D Program of China under Grant No. 2017YFE0300400 and the National Natural Science Foundation of China under Grant No. 11775257.

DATA AVAILABILITY

The data that support the findings of this study are available from the corresponding author upon reasonable request.

REFERENCES

[1]J. R. Myra and D. A. D'Ippolito, Phys. Plasmas **22**, 062507 (2015).
[2]Y. Zhang, J. Liu, Y. Liu, and X. Wang, Phys. Plasmas **11**, 3840 (2004).
[3]N. Xiang, Phys. Plasmas **11**, 4213 (2004).
[4]N. Xiang, Y. Hu, and J. Ou, Plasma Sci. Technol. **13**, 385 (2011).
[5]S. Bieher, J. Appl. Phys. **54**, 317 (1989).
[6]E. A. Edelberg and E. S. Aydil, J. Appl. Phys. **86**, 4799 (1999).
[7]D. Bose, T. R. Govindan, and M. Meyyappan, J. Appl. Phys. **87**, 7176 (2000).
[8]Z. L. Dai, Y. N. Wang, and T. C. Ma, Phys. Rev. E **65**, 036403 (2002).
[9]D. C. Kwon, M. Y. Song, and J. S. Yoon, J. Phys. D **46**, 025202 (2013).
[10]X. An, J. Ou, and Z. Men, Plasma Sci. Technol. **22**, 065103 (2020).
[11]J. Ou, X. An, and Z. Men, Phys. Plasmas **26**, 123514 (2019).
[12]L. Schott, Phys. Fluids **30**, 1795 (1987).
[13]T. Gyergyek, J. Kovacic, and M. Cercek, Phys. Plasmas **17**, 083504 (2010).
[14]G. Foroutan and A. Akhoundi, Phys. Plasmas **19**, 103505 (2012).
[15]J. Ou, X. Zhao, and C. Gan, Phys. Plasmas **23**, 043510 (2016).
[16]A. Arghand-Hesar, A. Esfandyari-Kaleijahi, and M. Akbari-Moghanjoughi, Phys. Plasmas **24**, 063504 (2017).
[17]J. Ou, N. Xiang, and Z. Men, Phys. Plasmas **25**, 012509 (2018).
[18]S. Basnet and R. Khanal, Phys. Plasmas **26**, 043516 (2019).
[19]J. I. Jauberteau and I. Jauberteau, Contrib. Plasma Phys. **51**, 944 (2011).
[20]N. Navab Safa, H. Ghomi, and A. R. Niknam, Phys. Plasmas **21**, 082111 (2014).
[21]O. Bouzit, L. A. Gougam, and M. Tribeche, Phys. Plasmas **22**, 052112 (2015).
[22]H. Khalilpour and V. Foroutan, Contrib. Plasma Phys. **60**, e201900060 (2020).
[23]C. Tsallis, J. Stat. Phys. **52**, 479 (1988).
[24]M. P. Leubner, Astrophys. Space Sci. **282**, 573 (2002).
[25]R. A. Cairns, A. A. Mamun, R. Bingham, R. Boström, R. O. Dendy, C. M. C. Nairn, and P. K. Shukla, Geophys. Res. Lett. **22**, 2709, https://doi.org/10.1029/95GL02781 (1995).
[26]M. Tribeche, R. Amour, and P. K. Shukla, Phys. Rev. E **85**, 037401 (2012).
[27]G. Williams, I. Kourakis, F. Verheest, and M. A. Hellberg, Phys. Rev. E **88**, 023103 (2013).
[28]S. Guo and L. Mei, Phys. Plasmas **21**, 082303 (2014).
[29]A. A. Abid, M. Z. Khan, S. L. Yap, H. Tercas, and S. Mahmood, Phys. Plasmas **23**, 013706 (2016).
[30]M. Farooq, A. Mushtaq, and M. Shamir, Phys. Plasmas **25**, 122110 (2018).
[31]W. F. El-Taibany, N. M. El-Siragy, E. E. Behery, A. A. El-Bendarb, and R. M. Taha, Chin. J. Phys. **58**, 151 (2019).
[32]D. Darian, S. Marholm, M. Mortensen, and W. J. Miloch, Plasma Phys. Controlled Fusion **61**, 085025 (2019).
[33]T. I. Rajib, N. K. Tamanna, N. A. Chowdhury, A. Mannan, S. Sultana, and A. A. Mamun, Phys. Plasmas **26**, 123701 (2019).
[34]F. Verheest and S. R. Pillay, Phys. Plasmas **15**, 013703 (2008).
[35]J. Gierling and K.-U. Riemann, J. Appl. Phys. **83**, 3521 (1998).
[36]N. Franklin, J. Phys. D **36**, R309 (2003).
[37]K. U. Riemann, IEEE Trans. Plasma Sci. **23**, 709 (1995).
[38]M. A. Lieberman, IEEE Trans. Plasma Sci. **16**, 638 (1988).
[39]M. Bures, J. J. Jacquinot, M. F. Stamp, D. D. R. Summers, D. F. H. Start, T. Wade, D. A. D'Ippolito, and J. R. Myra, Nucl. Fusion **32**, 1139 (1992).
[40]G. Urbanczyk, X. J. Zhang, L. Colas, A. Ekedahl, S. Heuraux, J. G. Li, C. M. Qin, Y. P. Zhao, L. Zhang, and X. D. Yang, Nucl. Mater. Energy **17**, 274 (2018).
[41]X. Zhang, F. K. Liu, Y. P. Zhao, J. F. Shan, B. J. Ding, C. M. Qin, M. Wang, H. D. Xu, X. J. Wang, M. H. Li, X. Z. Gong, L. Q. Hu, B. N. Wan, Y. T. Song, and J. G. Li, "The main experimental results and challenges in the ICRF heating on EAST," 23rd Topical Conference on Radiofrequency Power in Plasmas, Hefei, China, May 14–17 (2019).
[42]T. G. Jenkins and D. N. Smithe, Plasma Sources Sci. Technol. **24**, 015020 (2014).

Published under license by AIP Publishing